Int. J. Radiation Oncology Biol. Phys., Vol. 18, pp. 895–902
Printed in the U.S.A.

0360-3016/90 $3.00 + .00

● *Original Contribution*

EVALUATION AND OPTIMIZATION OF THE ELECTROMAGNETIC PERFORMANCE OF INTERSTITIAL ANTENNAS FOR HYPERTHERMIA

M. F. ISKANDER, PH.D., A. M. TUMEH, M.S. AND C. M. FURSE, M.S.

Electrical Engineering Department, University of Utah, Salt Lake City, Utah 84112

Effective and realistic evaluation of the performance of interstitial antennas for microwave hyperthermia involves: (a) calculations of the radiation characteristics of these antennas, including those of multi-section designs, and (b) the development of 3-dimensional models of tumors and the computation of the power deposition patterns in these tumors due to their irradiation by an array of interstitial antennas. In this paper, we address both of these issues. Specifically, we developed numerical models for calculating the radiation characteristics of multi-section insulated antennas, and we utilized a 3-dimensional model based on a volume integral equation formulation for calculating the power deposition pattern in tumors. Numerical results were verified by comparing them with experimental data available in the literature. New numerical data are presented to illustrate the advantages of multi-section designs over uniformly-insulated interstitial antennas and to show the feasibility of using amplitude and phase steering capabilities to control the power deposition patterns of an interstitial antenna array. The role of each section in a multi-section antenna design in guiding versus radiating the electromagnetic energy and hence in controlling the power deposition pattern of multi-section antennas is also described.

Interstitial antennas, Hyperthermia, Microwave hyperthermia.

INTRODUCTION

In microwave hyperthermia the use of interstitial antennas, particularly in an array form, has recently gained popularity. This is because this type of antenna applies heat directly to tumors and can heat deep-seated tumors with minimum temperature rise in surrounding tissues. It is also relatively easier to control the heating patterns of these antennas using an array system. In some designs, these antennas have thermistors mounted in them and may therefore provide temperature measurements simultaneously with the application of microwave radiation. The increased popularity of interstitial antennas for microwave hyperthermia has resulted from the spread utilization of ionizing radiation treatments using brachytherapy, where ribbons of irridium-192 are inserted into catheters during interstitial radiation therapy.

For realistic and effective evaluation of the performance of interstitial antennas for microwave hyperthermia, the radiation characteristics of these antennas, including those involving multi-section designs, must be accurately modeled and evaluated, and a 3-dimensional (3D) model for calculating the power deposition pattern in tumors should be developed. In the 3D model, accurate modeling of the tumor's geometry, as well as the differential changes in its properties as compared to those of the host tissue, must be accommodated.

In this paper we address these issues and present numerical results showing the power deposition patterns of multi-section insulated antennas in 3D models of tumors of various sizes. In the following sections we will describe the developed numerical models for calculating the radiation characteristics from interstitial antennas including those of multi-section design, and for computing the electromagnetic power deposition in 3-dimensional tumor models. Results illustrating the advantages of using multi-section designs and the role of the various sections in a given design in controlling the power deposition pattern are shown. The feasibility of controlling the radiation patterns using magnitude and phase steering in an interstitial array system is also described.

METHODS AND MATERIALS

Radiation characteristics of interstitial antennas

Interstitial antennas are basically uniformly-insulated or multi-section insulated antennas immersed in the conductive medium of tissue. These antennas are end-fed by coaxial transmission lines and may hence be approxi-

Reprint requests to: Magdy F. Iskander.
Acknowledgements—The authors are indebted to the reviewers of this manuscript, whose constructive recommendations contributed to the value and the clarity of the paper.

Accepted for publication 12 October 1989.

mately treated as monopole antennas. The calculation of the radiation characteristics of these antennas involves two major steps. The first is related to modeling and calculating the current and the charge distributions along the antenna, whereas the other is related to the calculation of the radiation fields in the conductive medium. These two topics will be treated separately in the following two sections.

1. *Current and charge distributions along insulated antennas.* Consider the multi-section monopole antenna shown in Figure 1. The current distribution along this antenna may be calculated based on the theory developed by King *et al.* (7, 8) for insulated antennas in conductive media. One of the most important conclusions of King's theory is that insulated antennas radiating in a conductive medium may be treated as sections of transmission lines with a complex propagation constant that accounts for the ohmic losses in conductors as well as for the radiation and coupling losses to the conductive ambient medium. Hence, for the multi-section design shown in Figure 1, the current distribution is given by:

$$I^i(z) = I^i_z(O)\frac{\sinh[k^i_L(h_i - |z|) + j\theta_i]}{\sinh[k^i_L h_i + j\theta_i]} \qquad (1)$$

$$I^i_z(o) = V_o/Z^i_{in}$$

and

$$Z^i_{in} = -jZ^i_C\coth(k^i_L h_i + j\theta_i),$$

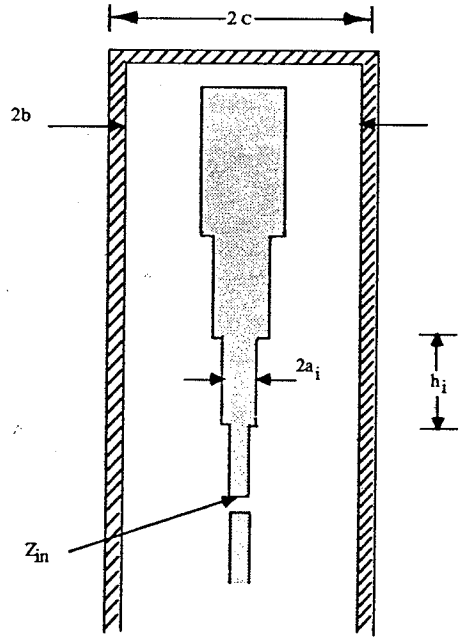

Fig. 1. Geometry of the multi-section monopole antenna. 2c and 2b are the outer and inner diameters, respectively, of the insulation; $2a_i$ and h_i are the diameter and length, respectively, of the center conductor of the ith section in the multi-section design.

where k^i_L is the complex propagation constant in the ith section, h_i is the length of the ith section, and θ_i is the angle that accounts for the loading effect of the ith section by the (i − 1)th section. θ_i is given by

$$\theta_i = \coth^{-1}(Z^{(i-1)}_{in}/Z^i_C),$$

where $Z^{(i-1)}_{in}$ is the input impedance of the (i − 1)th section that terminates the ith section of characteristic impedance Z^i_C. Equation 1 may be used sequentially starting from the top section of the antenna and moving toward the input port. Hence the input impedance and the current distribution along the antenna will account for the loading effects of the multiple sections all the way to the top end of the antenna. The tip of the antenna may be considered open- or short- (center and outer conductors of the coaxial feed are joined at the tip (13)) circuit, depending on the specific design of the antenna (12). The charge distribution along the antenna may be calculated using the continuity equation

$$q = \frac{j}{\omega}\frac{dI}{dz}. \qquad (2)$$

Note that the analysis presented in this section is based on King's theory (7, 8) and hence the expressions for the characteristic parameters of the antenna including the propagation constant k^i_L, the characteristic impedance Z^i_C, and the input impedance Z^i_{in} in terms of the dimensions of the antenna sections and the thickness and type of the catheter insulation are available elsewhere (6, 7, 8). These parameters are summarized for convenience in Appendix A for the ith section as related to the geometry of Figure 1.

Procedures for calculating the radiation fields in the ambient media from the current and charge distributions will be described in the following sections.

2. *Rigorous theory for calculating the radiation fields.* In this procedure we extend the analysis described by King *et al.* (8) to the case of multi-section antennas. First we utilize quasi-static bases to relate the current and charge distributions along the monopole antenna to the magnetic- and electric-field intensities in the insulation region. Hence

$$H_\phi = \frac{I(z)}{2\pi\rho}$$

$$E_\rho = \frac{q(z)}{2\pi\epsilon_e\rho}$$

$$E_z = \int_a^\rho \left[\frac{dE_\rho}{dz} + j\omega\mu_o H_\phi\right]d\rho.$$

In these expressions, the radiation from the end of the antenna was neglected, and the two regions (air and teflon catheter) separating the center conductor from the am-

bient were replaced by an equivalent dielectric medium of ϵ_e (8). The boundary conditions were then used to relate the various electric- and magnetic-field components within the insulation to the outside surface of the catheter. The electric field at any point (ρ, z) in the ambient conductive medium may then be determined in terms of the electric $E_\rho(c, z')$, $E_z(c, z')$, and the magnetic $H_\phi(c, z')$ field components at the surface of the insulation $\rho = c$, by

$$\bar{E}(\rho, z) = \frac{1}{4\pi}\int_0^h dz' \int_{-\pi}^{\pi} cd\phi' \left[-j\omega\mu_0 H_\phi(c, z')\frac{e^{-jk_4R}}{R}\bar{i}_z\right] - E_z(c, z')\bar{i}_\phi \times \nabla'\left(\frac{e^{-jk_4R}}{R}\right) + E_\rho(c, z')\nabla'\left(\frac{e^{-jk_4R}}{R}\right), \quad (3)$$

where c is the radius of the insulation, and $R = \sqrt{(\rho - \rho')^2 + (z - z')^2}$ is the distance from the equivalent source point (ρ', z') to the observation point (ρ, z). k_4 is the wave number in the ambient medium. Since several interstitial antennas involve multi-section designs, the length h of the antenna is divided into N portions

$$h = \sum_{i=1}^{N} h_i,$$

and the integration in Eq 3 is carried out over these various N sections. Note that in addition to having a different length for each section, the current and charge distributions, the propagation constant k_L^i and the characteristic impedance Z_C^i are also different for each section. Separate expressions for these quantities in terms of the dimensions of the antenna and the insulation may be obtained from the formulas given in Appendix A. Furthermore, the continuity of the current and charge distributions throughout the various sections should be enforced.

To validate the accuracy of the developed numerical code, we artificially divided a uniformly-insulated antenna, for which the results by King *et al.* (8) are available, into three sections and compared the obtained results with those available in the literature (8). Figure 2 shows a comparison between the results from the multi-section code and the available data for uniformly-insulated antennas. In general, good agreement is observed at the two radial distances for both the axial E_z and radial E_ρ field components as shown in Figure 2. Other validations for the current distribution and the input impedance results were also performed and excellent agreement was observed. Figure 3 shows comparison of the input impedance results for a uniformly-insulated antenna. Once again, the results from the multi-section code were obtained by artificially dividing the antenna into three sections of equal lengths. Figure 3 shows the comparison between numerical results obtained from the theory of uniformly-insulated antennas and the multi-section code. The comparison between numerical and experimental results is shown elsewhere.

The following section describes an approximate numerical model for calculating the radiation fields from multi-section antennas.

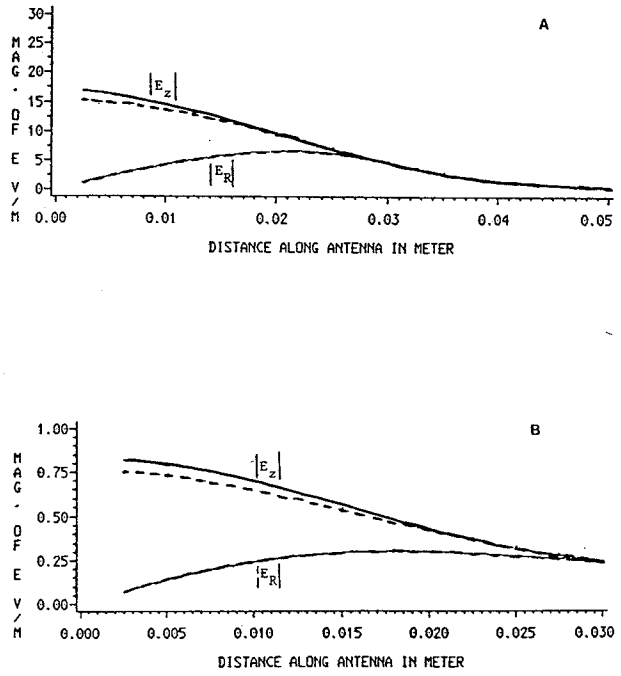

Fig. 2. Comparison between the results from the multi-section code (three sections) and the available data for a uniformly-insulated antenna. Figure 2a shows the results for calculations made at radial distance R = 1 cm from the surface of the insulation, and Figure 2b shows results at radial distance R = 3 cm from the surface of the insulation. The half length of the antenna in Figure 2a is h = 3.1 cm, whereas the half length in Figure 2b is h = 1.55. The dielectric properties of the ambient $\epsilon_4 = 42.5$, and $\sigma_4 = 0.88$ at 915 MHz, and the dielectric constant of the insulation $\epsilon_{r3} = 1.78$, 2a = 0.94 mm, 2b = 1.168 mm, and 2c = 1.6 mm, $k_L = 50.6 + j10.7\ m^{-1}$, $Z_c = 71.4 + j16.3\Omega$. $|E_z|$ and $|E_R|$ are the magnitudes of the axial and radial components, respectively, of the electric field.

3. *Approximate model for calculating the radiation characteristics of multi-section insulated antennas.* In this model we still use the current and charge distributions as

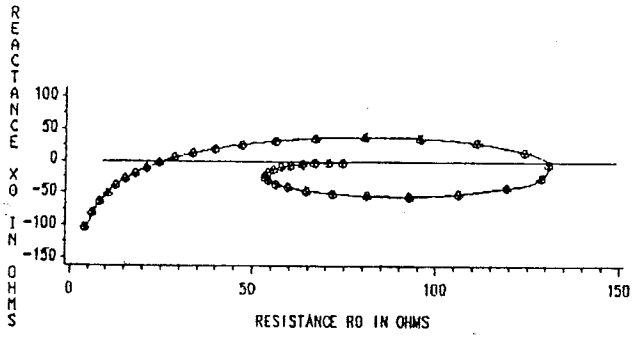

Fig. 3. Comparison of the input impedance $Z_o = R_o - jX_o$ results of a uniformly-insulated antenna: × = Results from King *et al.* (8); ○ = Results from the multi-section code. The dimensions of the antenna are as follows: 2a = 0.94 mm, 2b = 1.168 mm, and 2c = 1.6 mm. The calculations were made at 915 MHz and as a function of length. The length h was varied from h = 1 cm to h = 10 cm; $k_L = 50.6 + j10.7\ m^{-1}$, $Z_c = 71.4 + j16.3\Omega$.

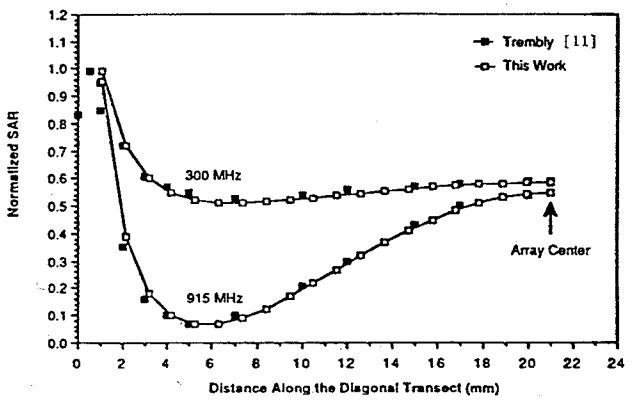

Fig. 4. Normalized specific absorption rate (SAR) for an array of a 3-cm square, four-element, uniformly-insulated antenna. The results from the approximate model described in this paper were compared with data from the rigorous theory developed for uniformly-insulated antennas.

described in Section 1. Calculation of the radiation characteristics, however, was based on a discrete point-source distribution on the surface of the insulation. The amplitude of these point sources is proportional to the amplitude (magnitude and phase) of the current at the location of the point source. To further account for the radiation capability of each section of the antenna, the amplitude of the point source was multiplied by what we called the "radiation efficiency factor," α_i/β_i, where α_i and β_i are the real and imaginary parts of the complex propagation constant $k_L^i = \alpha_i + j\beta_i$ in the ith section of the antenna. Note that the factor α/β is proportional to the energy losses (radiation plus ohmic losses) per wavelength. The introduction of this α/β factor was found important in improving the accuracy of the calculated radiation fields very near the antenna.

After establishing the point-source distribution with the appropriate amplitudes along the antenna, the radiation fields at any point in the ambient medium are calculated as the vector sum of the fields from each one of the point sources. The radiation fields from each point source are those usually used for infinitesimal electric dipoles (4).

Figure 4 shows comparison of the results obtained using this approximate model and the exact theory (4) for an array of four uniformly-insulated antennas. The results shown in Figure 4 are for the specific absorption rate (SAR) distribution along the transect of the 3-cm square, four-element array. Good agreement is observed even for distances as close as 1 mm from the surface of the insulation.

Figure 5 shows results of two comparisons between numerical and experimental data for commercially available multi-section antennas. Comparisons are shown for two commercially available antennas*. The numerical results were obtained based on the point-source distribution approximate model, whereas the experimental data were published in (10). Good agreement is observed even for the complicated design of the five-section interstitial antennas† (3).

Three-dimensional modeling of tumors

In the previous sections, numerical models were developed to calculate the radiation characteristics of interstitial antennas in a homogeneous ambient medium. For accurate determination of the SAR distribution in tumors, however, it is important to develop 3D models that account for the geometry of the tumor as well as for the difference in its dielectric properties as compared to those of the host tissue. We developed such a 3D model and made SAR calculations in small and large tumors in a host brain tissue (3). The 3D model is based on a volume integral equation formulation and the method of moments was used to obtain the solution (9). The incident fields were calculated from an array of interstitial antennas which are assumed to be sufficiently far apart to neglect the mutual coupling and sufficiently insulated to neglect the influence of the scattered fields on the current distribution along the antenna (3). The accuracy and the convergence of the 3D model as well as the validity of the various incident field assumptions are described in detail elsewhere (3). Specifically, it is noted that the mutual coupling between the array elements may be neglected if the antennas are placed at a distance 3 cm apart at 915 MHz, and that the effect of the scattered fields on the current distribution along the antenna may be neglected if the ratio of the insulation to center conductor diameters is more than 1.5, which is also easy to achieve using typical clinical antennas. Also, for the purpose of SAR calculations in the 2-cm diameter tumor, the tumor volume was discretized into 264 mathematical cells in each of which the induced electric field is assumed constant. After solving for the field components in these cells using the procedure described in (3), the SAR distribution is then calculated based on the magnitude of the fields in these mathematical cells.

In the following section we present new results that illustrate the SAR pattern-steering capabilities of an interstitial antenna array, and the advantages of multi-section designs over uniformly-insulated antennas.

RESULTS

Among the most significant advantages of using an array of interstitial antennas for microwave hyperthermia is the ability to heat the tumor in a localized and controlled fashion. Figure 6 shows the geometrical arrangement of the array of four antennas used in calculating the results

* Including the BSD Medical and the Cheung 2-node interstitial antennas.

† BSD Medical.

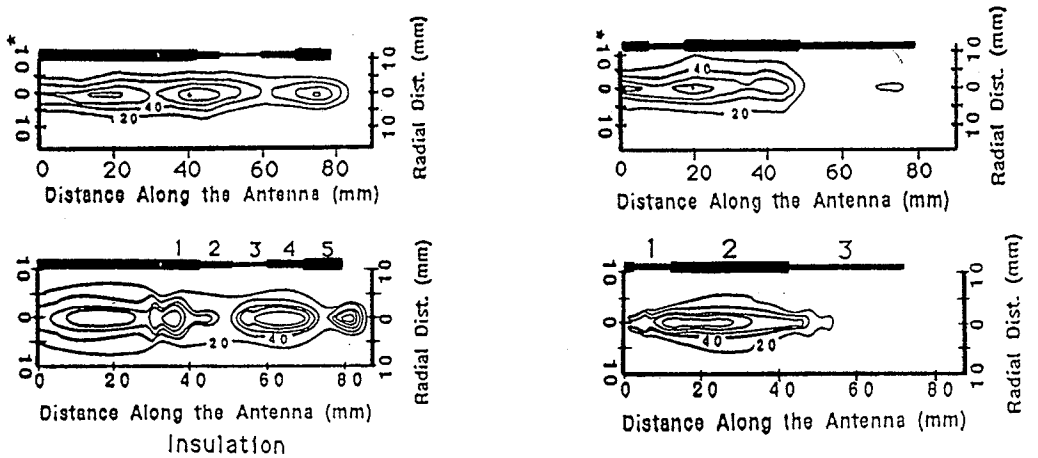

Section No.	1	2	3	4	5
α/β	0.217	0.203	0.139	0.203	0.217

Section No.	1	2	3
α/β	0.139	0.209	0.139

Fig. 5. Comparison between the numerical and experimental results of the power deposition pattern of two types of commercially available interstitial antennas ((a) the BSD Medical and (b) the Cheung 2-node interstitial antennas). Both patterns were calculated in a muscle-equivalent phantom of conductivity σ = 1.3 mho/m and dielectric constant ϵ_r = 50 at 915 MHz. The catheter size is 2.2 mm O.D. and 1.2 mm I.D. The experimental results are those reported by Ryan and Strohbehn (10) and indicated by an asterisk.

shown in Figures 7 and 8. Figure 6 also shows the various planes, that is, z = 0, z = 0.3125 cm, and z = 0.625 cm, at which the SARs in a spherical tumor are shown in Figures 7 and 8. Figure 7 shows the power deposition pattern in a 2-cm diameter spherical tumor as a result of its radiation using a 3-cm square, four-element array of uniformly-insulated antennas. The radii of the center conductor and the insulation are a = 0.333 mm and b = 1.0 mm, respectively. The monopole height is h = 3.47 cm, and the radiation frequency is 915 MHz. The increased conductivity in the tumor was based on results reported elsewhere (1). Figure 7a shows the power deposition pattern of the synchronous array, whereas Figure 7b shows the pattern when one of the elements was fed

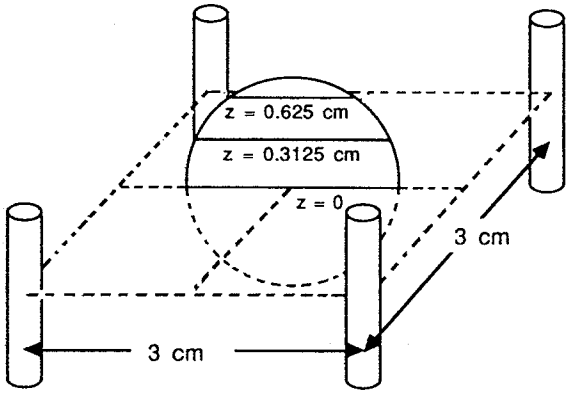

Fig. 6. Schematic illustrating the geometrical arrangement of the four-element array of interstitial antennas used to make calculations reported in Figures 7 and 8. Shown also is the location of the planes z = 0, z = 0.3125 cm, and z = 0.625 cm at which the SAR patterns are shown in Figures 7 and 8.

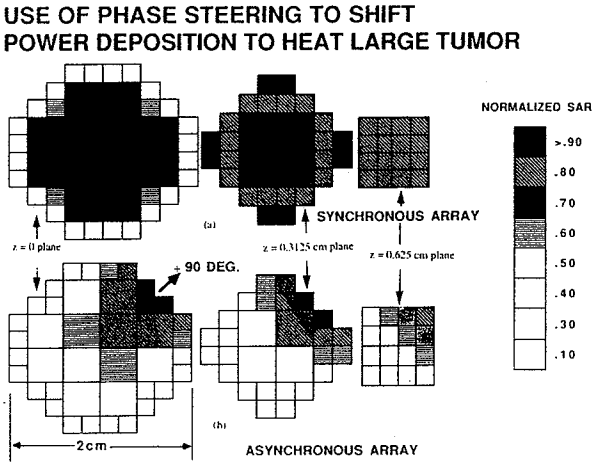

Fig. 7. The specific absorption rate (SAR) distribution in a 2-cm diameter tumor due to its irradiation by a 3-cm square, four-element array. Results are shown at the three planes shown schematically in Figure 6. The dielectric constant and conductivity of the ambient are ϵ_{r4} = 42, σ_4 = 0.88 S/m, respectively at 915 MHz, whereas the dielectric constant and conductivity of the tumor were taken to be ϵ_r = 55 and σ = 1.45 S/m, respectively. (a) Results for the synchronous array; (b) Results for an array when one of the elements (right-hand, top-corner element) has 90° phase lead relative to the others.

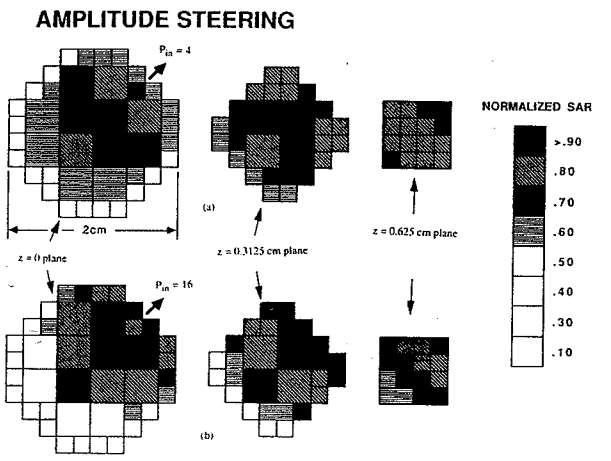

Fig. 8. SAR pattern in a 2-cm diameter tumor due to its irradiation by a 3-cm square, four-element array. Results are shown at the three planes schematically illustrated in Figure 6. The dielectric parameters are the same as those given in Figure 4. (a) One element (top right-hand element) has input voltage double that of the rest; (b) The same element has 4 times the input voltage of the other array elements.

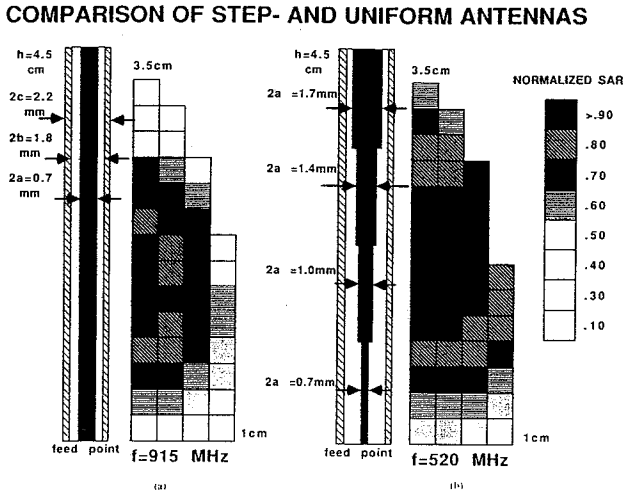

Fig. 9. SAR distribution in a spheroidal model of tumor. The semi-major and semi-minor axes are 3.5 cm and 1 cm, respectively. The multi-section design, while of the same length h = 4.5 cm as the uniformly-insulated one, achieved good impedance matching at lower frequency 520 MHz instead of 915 MHz. Figure 7b shows an improved SAR distribution along the antenna (as compared to Figure 7a) and improved depth of penetration.

by a 90° phase leading voltage. Figure 7a illustrates the fact that for larger tumors, 2 cm in diameter or greater, a difference of 50% may be observed for the SAR values at the core and the periphery of the tumor. Figure 7b shows the results with the 90° phase shift in one element and suggests a sequential heating process for achieving a uniform power deposition in the 2-cm diameter tumor. The core may be heated first using the synchronous array. The periphery may then be heated sequentially in four sections by shifting the phase of one element at a time by 90°. The results shown in Figure 7 show an effective means for controlling the heating pattern since a 90° phase shift in one of the elements steered the SAR pattern a distance of 1 cm from the core to the periphery of the tumor.

Figure 8 shows the results of a similar attempt to steer the heating pattern by varying the relative amount of the input power to the various array elements. Figure 8a illustrates the changes as a result of making the input power in one element in the array four times larger than the input power in the others, whereas Figure 8b shows a significant steering of the SAR pattern after changing the input power in one element of the array to 16 times the input power of the other elements. Figure 8 clearly illustrates the feasibility of steering the SAR pattern using the power rather than the phase of the input voltage. By comparing Figures 7 and 8, however, one may see that it is relatively easier to use phase rather than magnitude steering. It is generally known that achieving a 16:1 power ratio is more difficult than changing the phase (particularly over a narrow band of frequencies) by 90°. Both options, however, provide flexibility in steering the heating pattern to achieve desirable controls.

Many interstitial antennas involve the utilization of multi-section designs. These designs are intended to improve the heating pattern along the antenna and to lower the resonant frequency for a given physical antenna size and hence improve the depth of penetration of the microwave energy in the tissue. We have utilized the numerical model developed to design and optimize the performance of multi-section interstitial antennas (5, 12). The accuracy of the numerical model was verified by comparing the numerical results with experimental data available on commercially available antennas.‡ Some of these comparison results were shown in Figures 4 and 5 to illustrate the accuracy of the developed numerical model. All the results reported in our previous publications (5, 12) however, were for radiation in homogeneous tissue surrounding the antenna. In this section we compare the performance of uniformly-insulated and multi-section antennas in a spheroidal model of a tumor of 3.5 cm and 1 cm semi-major and semi-minor axes, respectively. The SAR distribution that resulted from a 3-cm square, four-element array is shown in Figure 9. Figure 9a illustrates the SAR pattern obtained from the uniformly-insulated antenna design of monopole length h = 4.5 cm. The dimensions of the antenna are 2a = 0.7 mm, 2b = 1.8 mm, and 2c = 2.2 mm. The input impedance of this antenna at 915 MHz when placed in an ambient of $\epsilon_r = 42.5$ and $\sigma = 0.88$ is $Z_{in} = 60 + j\ 33\ \Omega$, which may be considered reasonably matched to the feed 50 Ω coaxial line. A multi-section design of the same physical length h = 4.5 cm but of good impedance matching properties $Z_{in} = 52 - j\ 1.4$

‡ Such as the Dartmouth D9, BSD Medical, and Cheung antennas.

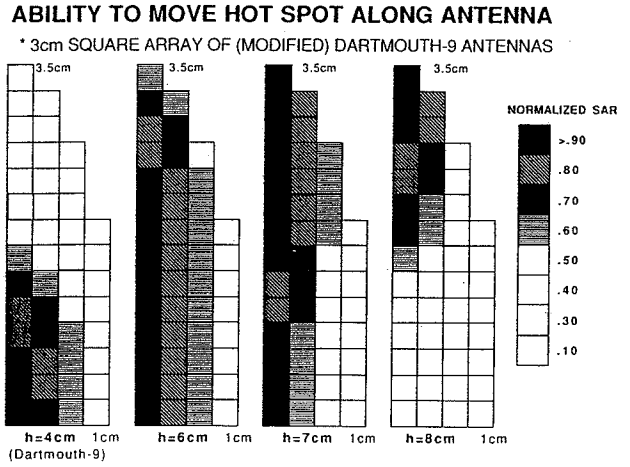

Fig. 10. SAR distribution in a spheroidal model of tumor for four different antenna lengths.

Ω at the much lower frequency of 520 MHz is shown in Figure 9b. This design basically consists of four sections of equal length and of varying diameters of the center conductor. Note that while the antenna length is h = 4.5 cm, the SAR distribution is shown only in a cross section of the spheroidal model of a tumor of 3.5 cm and 1 cm semi-major and semi-minor axes, respectively. The SAR pattern shown in Figure 9b has the following advantage over that of the uniformly-insulated antenna shown in Figure 9a:

1. It is more uniformly distributed along the antenna. This may be attributed to the ability of the intermediate sections of the antenna to guide (smaller α/β) rather than radiate (larger values of α/β) the electromagnetic energy to the ambient.
2. An improved depth of penetration may also be observed in Figure 9b as compared to Figure 9a. The increase in the depth of penetration in Figure 9b may be attributed to the lower operating frequency of the multi-section design, f = 520 MHz instead of 915 MHz.

A variety of other multi-section designs, the improvement in their power deposition patterns, and the role of the various sections in guiding versus radiating the electromagnetic energy are discussed in earlier publications (2, 5, 12).

Another observation that may be seen from Figure 9 is that the SAR pattern does not have its peak value at the feed region of the antenna. This is true for both the uniformly-insulated and multi-section antennas. To clarify the reason for this behavior, we computed the SAR for several uniformly-insulated antennas of different lengths varying from 4 to 8 cm at 915 MHz. The obtained results are shown in Figure 10, where it is clear that changing the antenna length may result in moving the SAR pattern along the antenna. Once again, the SAR distribution was plotted in a spheroidal model of a tumor of semi-major axis of 3.5 cm and semi-minor axis of 1 cm. Further examination of the reasons for this behavior showed that the SAR pattern closely resembles the current distribution along the antenna. Therefore, for antennas of length $h \leq \lambda_L/4$ where $\lambda_L = 2\pi/\beta$ and β is the imaginary part of the propagation constant k_L, we expect a maximum current at the feed point of the antenna and hence the SAR pattern to be near the feed region. As the antenna length approaches $h \leq \lambda_L/2$, the peak of the current distribution shifts towards the tip, and hence the SAR pattern, approach the tip of the antenna.

CONCLUSIONS

Numerical models for calculating the radiation characteristics of interstitial antennas in inhomogeneous tissue have been developed. The models may be used to calculate the radiation characteristics from multi-section antenna designs and may also account for the geometry of the tumor and the difference in its dielectric properties as compared to those of the host tissue. The accuracy of the obtained results were checked by comparing them with available data for the special case of a uniformly insulated interstitial antenna radiating in a homogeneous tissue and by comparing the power deposition pattern in a spherical tumor with data from the well-known Mie solution. The calculated radiation characteristics of multi-section insulated antennas were also compared with available experimental data (10, 12). In general, good agreement was observed and the accuracy of the developed numerical model was thus verified.

With the confidence developed in the numerical model, results were presented to illustrate the advantages of the multi-section antenna designs over the uniformly insulated interstitial antennas and to show the superior sensitivity of using the phase rather than the magnitude of the input voltages to the antenna array to steer the power deposition pattern over large tumors. This pattern steering capability was found to be very important in treating large tumors, since the difference between the core and the peripheral heating was found to be as much as 50%.

The developed numerical capabilities can now be used to design and optimize the radiation characteristics of interstitial antennas, including those of multi-section designs and also in evaluating their heating pattern in 3-dimensional models of tumors.

REFERENCES

1. Foster, K. R.; Schepps, J. L. Dielectric properties of tumor and normal tissues at radio through microwave frequencies. Jour. Mic. Power 16(2):107–119; 1981.
2. Furse, C. M.; Iskander, M. F. Three-dimensional electromagnetic power deposition in tumors using interstitial antennas. Presented at Tenth Annual Meeting of the Bioelectromagnetics Society, Stamford, CT, June 19–23, 1988.
3. Furse, C. M.; Iskander, M. F. Three-dimensional electromagnetic power deposition in tumors using interstitial antennas. IEEE Trans. BME (In press) 1989.

4. Harrington, R. F. Time-harmonic electromagnetic fields. New York, NY: McGraw-Hill; 1961.
5. Iskander, M. F.; Tumeh, A. M. Design optimization of interstitial antennas. IEEE Trans. BME. 36:238–246; 1989.
6. King, R. W. P.; Lee, K. M.; Wu, T. F. Theory of an insulated antenna in a desiccative medium. Radio Science. 12:195–203; 1977.
7. King, R. W. P.; Smith, G. S. Antenna in matter. Cambridge, MA: MIT Press; 1981.
8. King, R. W. P.; Trembly, B. S.; Strohbehn, J. W. The electromagnetic field of an insulated antenna in a conducting or a dielectric medium. IEEE Trans. MTT. MTT-31:574–583; July 1983.
9. Livesay, D.; Chen, K. M. Electromagnetic fields induced inside arbitrarily-shaped biological bodies. IEEE Trans. MTT. MTT-22:1273–1280; 1974.
10. Ryan, T. P.; Strohbehn, J. W. A comparison of power deposition for three microwave antennas used in hyperthermia cancer therapy. Presented at Ninth Annual Meeting of the Engineering in Medicine and Biology Society, Session on Electromagnetic Methods of Deep Heating, Boston, MA, November 13–16, 1987.
11. Trembly, B. S. The effect of driving frequency and antenna length on power deposition within a microwave antenna array used for hyperthermia. IEEE Trans. BME. BME-32: 152–157; 1985.
12. Tumeh, A. M.; Iskander, M. F. Performance comparison of available interstitial antennas for microwave hyperthermia. IEEE Trans. MTT. MTT-37:1126–1133; July 1989.
13. Turner, P. F. Interstitial equal-phased arrays for EM hyperthermia. IEEE Trans. MTT. MTT-34:572–578; May 1986.

APPENDIX A

According to the theory of insulated antennas developed by King *et al.* (6, 7, 8), these antennas, when placed in a conductive medium, may be treated as sections of transmission lines with a complex propagation constant that accounts for both the ohmic losses and the radiation losses to the ambient. For the ith section of the multisection design shown in Figure 1, the propagation constant is given by

$$k_L^i = k_2\left[\frac{\ln(c/a_i)}{\ln(b/a_i + n_{23}^2\ln(c/b)}\right]^{1/2}\left[\frac{\ln(c/a_i) + F}{\ln(c/a_i) + n_{24}^2 F}\right]^{1/2},$$

where

$$F = H_0^{(1)}(k_4c)/k_4cH_1^{(1)}(k_4c)$$

$$n_{23}^2 = k_2^2/k_3^2, \quad n_{24}^2 = k_2^2/k_4^2$$

$$k_2 = \omega\sqrt{\mu_0\epsilon_2}, \quad k_3 = \omega\sqrt{\mu_0\epsilon_3}, \quad \text{and} \quad k_4 = \omega\sqrt{\mu_0\epsilon_4^*}.$$

In Figure 1, $\epsilon_2 = \epsilon_0$ of air, $\epsilon_3 = \epsilon_0\epsilon_{r_3}$ where ϵ_{r_3} is the dielectric constant of the catheter material, and ϵ_4^* is the complex permittivity of the ambient.

$H_0^{(1)}$ and $H_1^{(1)}$ are the Hankel functions of the first kind and of the zeroth and first orders.

The characteristic impedance of the ith section is given by:

$$Z_C^i = \frac{\omega\mu_0 k_L^i}{2\pi k_2^2}[\ln(b/a_i) + n_{23}^2\ln(c/b) + n_{24}^2 F].$$

This analysis is subject to the constraints

$$|k_4/k_2|^2 \gg 1, \quad |k_4/k_3|^2 \gg 1$$

$$(k_2b)^2 \ll 1, \quad \text{and} \quad (k_3c)^2 \ll 1.$$